



**HAL**  
open science

## A validation strategy for LES subgrid scale models

Benedetta Franzelli, A. Vié, Denis Veynante

► **To cite this version:**

Benedetta Franzelli, A. Vié, Denis Veynante. A validation strategy for LES subgrid scale models. 10th European Combustion Meeting (2021), Apr 2021, Napoli (Virtual conference), Italy. hal-03407027

**HAL Id: hal-03407027**

**<https://hal.science/hal-03407027>**

Submitted on 2 Nov 2021

**HAL** is a multi-disciplinary open access archive for the deposit and dissemination of scientific research documents, whether they are published or not. The documents may come from teaching and research institutions in France or abroad, or from public or private research centers.

L'archive ouverte pluridisciplinaire **HAL**, est destinée au dépôt et à la diffusion de documents scientifiques de niveau recherche, publiés ou non, émanant des établissements d'enseignement et de recherche français ou étrangers, des laboratoires publics ou privés.

10<sup>TH</sup>  
EUROPEAN  
COMBUSTION  
MEETING

April 14-15, 2021

Virtual Edition



# PROCEEDINGS VOLUME

[www.ecm2021napoli.eu](http://www.ecm2021napoli.eu)



# A validation strategy for LES subgrid scale models

B. Franzelli<sup>a,\*</sup>, A. Vié<sup>a</sup>, D. Veynante<sup>a</sup>

<sup>a</sup>Laboratoire EM2C, Université Paris-Saclay, CNRS, CentraleSupélec,  
1-3 rue du Joliot Curie, 91960 Gif-sur-Yvette, France

## Abstract

Large eddy simulation (LES) of turbulent reacting flows relies on several models accounting for subgrid scale effects on flow dynamics, scalar transport, reaction rates or spray evolution for instance. In the literature, many subgrid approaches have been developed in the last decades based on *a priori* analysis of direct numerical simulations (DNS). Then, to be validated *a posteriori*, these models are generally directly used in LES of reference DNS or of experimental configurations. However, an actual LES combines several models enabling only the validation of the global LES strategy, but not of each individual model.

To overcome this issue, the present work proposes a rigorous *a posteriori* validation strategy based on the transport of a filtered scalar equation by unfiltered flow variables, so that the sole filtered quantity is the scalar itself. By solving these equations on a DNS-like grid, and using deconvolution algorithms, the effect of a single subgrid model can be analysed, while exactly evaluating the other terms. The proposed approach is illustrated investigating simple models to predict the propagation of a turbulent premixed flame.

## 1. Introduction

Large eddy simulation (LES) of turbulent reacting flows is today widely used to understand physics and behavior of actual realistic configurations, such as gas turbines or automotive engines. Because of the multiphysics character of such applications, several modelling components have to be combined to capture the whole physics, such as spray, combustion and turbulent dynamics. Furthermore, because of the filtering of the equations imposed by the LES, subgrid scale (SGS) models are needed to account for unresolved contributions.

Various formalisms have been proposed in the literature to model turbulent combustion in an LES context [1]. Whatever the model, the validation strategy is in general twofold: first, the model is evaluated *a priori* based on reference direct numerical simulations (DNS) (see [2–9] for instance). Second, the model is implemented in an LES corresponding to the reference DNS configuration or in a different configuration with other validation data [7, 10]. This second step rises two questions. First, in an LES, the model in sight is combined to other SGS models with their own modeling error. Therefore, the combination of all models can give satisfactory results, without ensuring that the model itself is correct. At a second level, an LES is in general performed with coarser meshes than DNS. Then, the competition between numerical scheme and modeling errors has to be analysed with great care.

To overcome these issues, we propose a strategy to validate subgrid scale models isolating their specific effects. As an example, this methodology is applied to the filtered reaction rates. To avoid competition between models, we propose to solve the balance equations of the filtered species mass fractions together with the unfiltered flow field equations (density, velocity, energy). By doing so, the flow field is fully resolved while the unresolved transport and diffusion terms in the species equations is evaluated from deconvoluted quantities, potentially giving access to the full information assuming

an exact deconvolution reconstruction. The filtered reaction rate is closed with the subgrid scale model to be tested. The performance of the model is then assessed by comparing in a statistical way the results to the filtered DNS fields without any possible interactions from other subgrid models. The simulations are performed on the DNS grid, considering an explicit filter whose width is specified by the user. By doing so, interactions between numerical scheme and model are minimized, as well as possible errors of the deconvolution algorithm due to sub-sampling of the solution.

The paper is organized as follows. In Sec. 2, the concept of the proposed validation strategy is presented. In Sec. 3, its feasibility is discussed on a simplified configuration, together with the necessary tools for filtering and deconvolution. In Sec. 4, the results are presented and the effect of the SGS models for the filtered reaction rate is discussed in terms of the statistical description of the resolved characteristics of the turbulent flame.

## 2. Theoretical formulation

Let us consider the fully-resolved mass fraction balance equation of a chemical species  $k$ :

$$\frac{\partial \rho Y_k}{\partial t} + \frac{\partial}{\partial x_i} (\rho u_i Y_k) = \frac{\partial}{\partial x_i} \left( \rho D_k \frac{\partial Y_k}{\partial x_i} \right) + \rho \dot{\omega}_k \quad (1)$$

where  $\rho$  and  $u_i$  are the gas density and velocity components,  $D_k$  is the molecular diffusivity, and  $\dot{\omega}_k$  is the chemical source term of species  $k$ .

In classical LES formulations, continuity, momentum and energy equations are filtered at the filter scale  $\bar{\Delta}$  together with the chemical species balance equation:

$$\frac{\partial \bar{\rho} \tilde{Y}_k}{\partial t} + \frac{\partial}{\partial x_i} (\bar{\rho} \tilde{u}_i \tilde{Y}_k) = \frac{\partial}{\partial x_i} (\bar{\rho} \tilde{u}_i \tilde{Y}_k - \overline{\rho u_i Y_k}) + \frac{\partial}{\partial x_i} \left( \bar{\rho} D_k \frac{\partial \tilde{Y}_k}{\partial x_i} \right) + \bar{\rho} \tilde{\omega}_k \quad (2)$$

where  $\bar{Q}$  and  $\tilde{Q} = \bar{\rho} \tilde{Q} / \bar{\rho}$  denote filtered and mass-weighted filtered quantities, respectively. The three right-hand side terms correspond to the unresolved transport,

\*Corresponding author: benedetta.franzelli@centralesupelec.fr



Approach	Transported variables	Species balance equation terms			
		Turb. Transp.	Diffusion	Reaction	Inter-scale convection
DNS	$\rho, \rho u_i, \rho Y_k$ (Eq. 1)	-	Fully resolved	Fully resolved	-
DNS2LES	$\rho, \rho u_i, \rho \tilde{Y}_k$ (Eq. 3)	Deconv. + Filt.	Deconv. + Filt.	Modeled	Fully resolved
LES	$\bar{\rho}, \bar{\rho} \tilde{u}_i, \bar{\rho} \tilde{Y}_k$ (Eq. 2)	Modeled	Modeled	Modeled	-

Table 1: Summary of the possible approaches for model validation. "Deconv." stands for deconvolution and "Filt." stands for filtering.

the filtered molecular diffusion and the filtered reaction rate. These terms require closures. Unresolved transport and filtered diffusion terms are usually modeled using a gradient-type closure [11]. Most of the efforts in the literature is devoted on the modeling of filtered reaction rates and the validation of the correspondent SGS models.

### 2.1. Strategy for the validation of subgrid scale models

The balance equation of the filtered variable  $\tilde{Y}_k$  together with the unfiltered balance equations for the other variables required by the model are considered. By analogy with the development proposed by Mercier et al. [12] regarding two different filter sizes in reactive LES, the transport equation of  $\tilde{Y}_k$  by  $\rho u$  is derived by combining Eq. (2) and the unfiltered total mass conservation:

$$\begin{aligned} \frac{\partial \rho \tilde{Y}_k}{\partial t} + \frac{\partial}{\partial x_i} (\rho u_i \tilde{Y}_k) = & \frac{\rho}{\bar{\rho}} \left[ \frac{\partial}{\partial x_i} (\bar{\rho} \tilde{u}_i \tilde{Y}_k - \overline{\rho u_i Y_k}) + \overline{\rho \dot{\omega}_k} \right] \\ & + \frac{\rho}{\bar{\rho}} \left[ \frac{\partial}{\partial x_i} \left( \overline{\rho D_k \frac{\partial Y_k}{\partial x_i}} \right) \right] + \rho (u_i - \tilde{u}_i) \frac{\partial \tilde{Y}_k}{\partial x_i} \end{aligned} \quad (3)$$

Right hand side of Eq. (3) contains the usual unresolved transport, reaction terms and diffusion, weighted by the density ratio  $\rho/\bar{\rho}$ . In addition, a new term accounting for inter-scale convection between DNS grid resolution and LES filter  $\bar{\Delta}$  is found. These terms can be evaluated following three strategies:

- They are computed from the DNS field once a physical filter  $F$  has been chosen. The transported  $\tilde{Y}_k$  is then strictly identical to the filtered  $Y_k$  from Eq. (1). This method is exact by construction and can be used only for *a priori* validation.
- All terms are closed by appropriate subgrid scale models, as similarly done in LES for Eq. (2). The specific contribution of each model cannot be isolated.
- The fully-resolved  $Y_k$  can be extracted from  $\tilde{Y}_k$  by deconvolution. Then, each term can be estimated either by a subgrid scale model or computed combining the knowledge of  $Y_k$  and the DNS flow fields. The specific case where only the filtered reaction term is closed by a subgrid scale model while all other terms are computed is considered here (case DNS2LES in Table 1). In this way, the effect of the filtered reaction rate model on the flame prediction can be isolated. Indeed, the obtained transported  $\tilde{Y}_k$  and the filtered  $Y_k$  from Eq. (1) are expected to be

statistically identical when the subgrid scale contributions are correctly modeled, assuming an accurate deconvolution reconstruction.

In conclusion, the DNS2LES strategy allows to introduce only one single subgrid scale model, as illustrated in Table 1. In this way, results will not be affected by the other subscale closures needed for the others terms of the species, mass, momentum and energy balance equations, as classically observed in *a posteriori* validation based on LES (see Table 1). This approach, here applied to the filtered reaction rate, can be similarly used to investigate the modeling of the other unresolved terms.

### 3. Proof of concept

The proposed validation strategy is illustrated considering the interaction between a premixed flame and an homogeneous isotropic turbulent (HIT) field. The flame front is described by a reaction progress variable  $c$ , evolving from fresh (0) to burnt (1) gases, with a reaction rate  $\dot{\omega}(c) = c(1-c)/\tau_c$ , where  $\tau_c$  is a given chemical time scale. In a first step, density and temperature are assumed constant decoupling turbulence and combustion. The equation system is composed by two unfiltered equations:

$$\frac{\partial \rho u_j}{\partial t} + \frac{\partial \rho u_i u_j}{\partial x_i} = -\delta_{ij} \frac{\partial P}{\partial x_i} + \frac{\partial \tau_{ij}}{\partial x_i} \quad (4)$$

$$\frac{\partial \rho c}{\partial t} + \frac{\partial \rho u_i c}{\partial x_i} = \frac{\partial}{\partial x_i} \left( \rho D \frac{\partial c}{\partial x_i} \right) + \rho \dot{\omega}(c) \quad (5)$$

and two equations for the filtered progress variable:

$$\begin{aligned} \frac{\partial \rho \tilde{c}_1}{\partial t} + \frac{\partial \rho u_i \tilde{c}_1}{\partial x_i} = & \frac{\partial}{\partial x_i} \left( \rho u_i \tilde{c}_1 - \overline{\rho u_i c_1^\dagger} \right) \\ & + \frac{\partial}{\partial x_i} \left( \overline{\rho D \frac{\partial c_1^\dagger}{\partial x_i}} \right) + \bar{\rho} \dot{\omega}(\tilde{c}_1) \end{aligned} \quad (6)$$

$$\begin{aligned} \frac{\partial \rho \tilde{c}_2}{\partial t} + \frac{\partial \rho u_i \tilde{c}_2}{\partial x_i} = & \frac{\partial}{\partial x_i} \left( \rho u_i \tilde{c}_2 - \overline{\rho u_i c_2^\dagger} \right) \\ & + 4\rho_u s_L \sqrt{\frac{6}{\pi}} \frac{\Xi}{\bar{\Delta}} \tilde{c}_2 (1 - \tilde{c}_2) \\ & + \frac{\partial}{\partial x_i} \left( \rho_u \frac{s_L \bar{\Delta}}{16 \sqrt{6/\pi}} \frac{\partial \tilde{c}_2}{\partial x_i} \right) \end{aligned} \quad (7)$$

where  $P$  is the pressure,  $\tau_{ij}$  the laminar stress tensor,  $Q^\dagger$  is the deconvolution of  $\rho \bar{Q}/\bar{\rho}$ ,  $\rho_u$  is the fresh gas density,  $s_L$  is the laminar flame speed,  $\Xi$  is the subgrid-scale flame front wrinkling factor.

The reference statistical behavior of the filtered quantities can be obtained by explicitly filtering the DNS solution  $c$  of Eq. (1) to get  $\tilde{c}$ . Equations (6) and (7) correspond to two different DNS2LES cases, allowing the



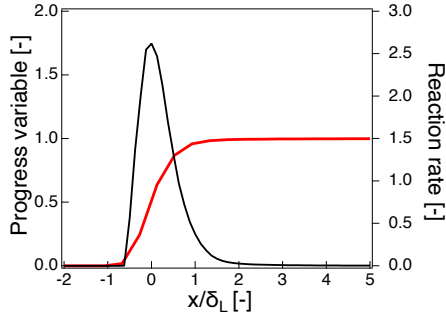


Figure 1: Progress variable (left scale) and reaction rate (right) initial profiles. The reaction rate has been made non-dimensional using  $\rho_u S_L / \delta_L$ .

evaluation of two subgrid scale closures for the filtered reaction rates when comparing the statistical behavior of  $\tilde{c}_1$  and  $\tilde{c}_2$  to the reference  $\tilde{c}$  behavior.

Equation (6) corresponds to the DNS2LES case without subgrid contribution to the reaction rate:  $\overline{\rho\dot{\omega}(c)} = \overline{\rho\dot{\omega}(\tilde{c})}$  (NO MODEL case).

Equation (7) evaluates a flamelet closure classically used in flame surface density concepts (BOGER case), where diffusion and reaction terms are modeled together [2]:

$$\nabla \cdot (\rho D \nabla c) + \overline{\rho\dot{\omega}_c} \approx \rho_u S_L \Sigma, \quad (8)$$

with  $\Sigma$  the flame surface density [13]:

$$\Sigma = 4 \sqrt{\frac{6}{\pi}} \Xi \frac{\tilde{c}(1-\tilde{c})}{\Delta}. \quad (9)$$

The subgrid-scale flame front wrinkling factor  $\Xi$  is here estimated from the subgrid turbulence rms velocity  $u'_{\Delta}$ :

$$\Xi = 1 + \frac{u'_{\Delta}}{S_L}. \quad (10)$$

More sophisticated models for  $\Xi$  are available in literature [14, 15].

### 3.1. Filtering and deconvolution

In the simulation, the filtering operation is performed using a truncated Taylor expansion [16, 17]:

$$\overline{Q} = Q + \frac{\Delta}{\gamma} \frac{\partial^2 Q}{\partial x_i^2} \quad (11)$$

where  $\gamma$  depends on the filter ( $\gamma = 24$  for a 1D Gaussian filter). The deconvolution algorithm is based on the Approximate Deconvolution Method (ADM) using Van Cittert series [18]:

$$Q^{\dagger, n+1} = Q^{\dagger, n} + b(\overline{Q} - \overline{Q^{\dagger, n}}), \quad \text{with } n = 0, N_t - 1 \quad (12)$$

where  $\overline{Q^{\dagger, 0}} = \overline{Q}$ ,  $N_t$  is the order of deconvolution and  $b$  is limited to ensure boundness of  $Q^{\dagger}$  [19]. Other deconvolution methods exist, such as the Regularized Deconvolution Method [20], or an implicit anti-diffusion process [17]. However, the ADM is the only viable choice using an explicit unstructured solver.

### 3.2. Numerical Setup

A turbulent premixed flame is simulated on a 2D grid of size 8 cm  $\times$  6 cm, discretized on  $N_x \times N_y = 1600 \times 1200$  points leading to cell size  $\Delta_m = 50 \mu\text{m}$ . A region of interest of size  $L_x \times L_y = 0.065 \text{cm} \times 0.05 \text{cm}$  is considered for the statistical analysis. The retained laminar flame speed is  $s_L = 0.4 \text{ m.s}^{-1}$ . To obtain a consistent description of the physical phenomena among the reference simulation and the NO MODEL and BOGER cases, the characteristics chemical time is chosen to be  $\tau_c = \Delta_m / (4 \sqrt{6} / \pi S_L) = 90 \mu\text{s}$  and a constant molecular diffusivity is assumed:  $\rho D = \rho_u s_L^2 \tau_c^{-1} / 4$ . To create the initial solution, a 2D premixed planar laminar flame is calculated. The obtained flame is characterized by a laminar flame thickness  $\delta_L = 1 / \max(|\nabla c|) = 0.4 \text{ mm}$ . The profiles of progress variable and source terms are illustrated in Fig. 1. The axial location is set to zero at the source term maximum to facilitate the analysis in the following. The simulation is performed with the AVBP solver, using the TTG4A scheme [21]. Non-reflecting inlet and outlet NSCBC conditions are applied in the x-direction, normal to the initial laminar flame. Adiabatic non-slip wall conditions are considered on top and bottom sides. Then, an homogeneous isotropic turbulent flow is injected at the left side, using a Passot Pouquet spectrum with the following characteristics: bulk velocity  $u_{\text{bulk}} = 4.5 \text{ m/s}$ , turbulent velocity  $u' = 3.5 \text{ m/s}$ , most energetic wave length  $\lambda_e = 5.0 \text{ mm}$ . The corresponding integral length scale is  $l_T = 12.5 \text{ mm}$ , the eddy turnover time is  $\tau_T = l_T / u' = 3.6 \text{ ms}$ , the convective time is  $\tau_{\text{conv}} = L_x / u_{\text{bulk}} = 17 \text{ ms}$ .

The simulation is performed over more than 15 eddy-turnover time to obtain a statistically steady turbulent flame. The instantaneous flame front at reduced time  $t^+ = t / \tau_T = 16$  is represented in Fig. 2 by looking at the c-isocontours colored by the reaction term together with the vorticity field. Due to the interaction with the turbulent flow, the flame is quite wrinkled, increasing its surface. Consequently, the consumption speed increases so that the flame, initially located close to the inlet injection, finally stabilizes in the middle of the domain. This solution represents the starting point for the following analy-

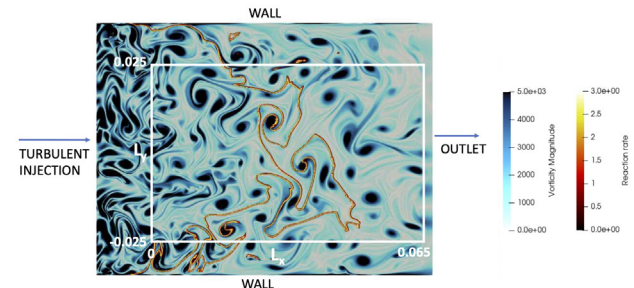


Figure 2: Instantaneous isocontours of progress variable colored by the reaction rate superimposed to the vorticity field at reduced time  $t^+ = 16$ . The reaction rate has been non-dimensionalized by  $\rho_u S_L / \delta_L$ . The white square of size  $L_x \times L_y$  indicated the region of interest considered for the statistical analysis.

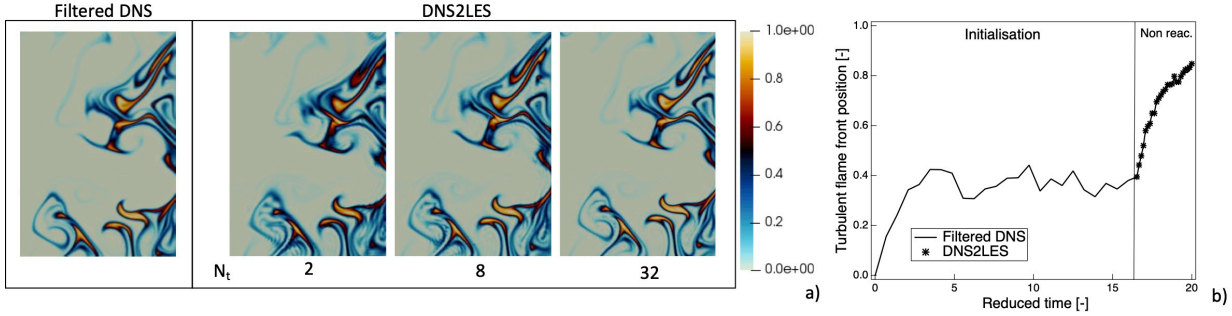


Figure 3: a) Instantaneous field for the progress variable at  $t^+ = 20$  for the non-reactive case. Reference filtered results from the DNS  $\tilde{c}$  are compared to the DNS2LES results  $\tilde{c}_1$  for  $N_t = 2, 8$  and  $32$ . b) Temporal evolution of the axial position of the mean turbulent flame front during the initialisation ( $t^+ < 16$ ) and the non-reactive ( $t^+ > 16$ ) calculations. The flame position has been made non-dimensional using the axial dimension of the region of interests,  $L_x = 0.065$  m. DNS2LES results are obtained with  $N_t = 32$ .

sis. The profile for the filtered variables are initialized by filtering  $c$  using a filter with  $\bar{\Delta} = 8\Delta_m \approx \delta_L = 0.4$  mm, which is a common LES grid size [16].

## 4. Results

### 4.1. Evaluation of the deconvolution procedure

Before evaluating the performances of the subgrid scale models, it is important to verify that the deconvolution procedure used to calculate the turbulent transport and the diffusion terms of Table 1 is not affecting the results. For this, a non-reactive case is considered by imposing  $\dot{\omega}(c)=0$  in Eqs. (5) and (6). When no reaction rate is considered, the progress variable is expected to be convected outside the domain by the turbulent flow. To calculate  $c_1^\dagger$  from  $\tilde{c}_1$ , an optimal value of the number of ADM iterations of  $N_t = 5$  is often suggested, based on the work of Stolz and Adams [22]. Here, three values have been considered:  $N_t = 2, 8$  and  $32$ . The instantaneous progress variable field is presented in Fig. 3a after four eddy turn-over times. The DNS field from Eq. (5) has been filtered and can be considered as the reference solution. For small values of  $N_t$  the solution  $\tilde{c}_1$  from Eq. (6) presents numerical oscillations, which are controlled for  $N_t = 32$ . For a sufficiently accurate deconvolution algorithm, solutions  $\tilde{c}$  and  $\tilde{c}_1$  should present the same statistical behavior. To confirm it, the temporal evolution of the axial position of the turbulent flame front is represented in Fig. 3b. This quantity has been obtained by spatially averaging at each instant the axial position of the flame front, identified by  $0.4 < \tilde{c} < 0.6$ . For this, only the region of interest of size  $L_x \times L_y$  indicated in Fig. 2 has been considered. As said, the laminar flame is initially localized at  $x = 0$  ( $t^+ = 0$ ). During the initialization of the computation ( $t^+ < 16$ ), the flame front is initially pushed downstream by the turbulent flow and finally stabilizes close to the middle of the domain after 5 eddy turn-over times. Once the reaction is put to zero ( $t^+ > 16$ ), the flame is rapidly convected towards the outlet and finally exists the domain. It can be observed that the DNS2LES results reproduce the same statistical behavior of the filtered DNS calculation, guaranteeing the fact that the the conclusions on the performances of the SGS models evaluated in the following will not be af-

ected by the reconstruction of the turbulent transport and diffusion terms from the filtered quantities.

### 4.2. Evaluation of the subgrid scale models

To quantify the impact of the subgrid scale models on the flame front characteristics, the simulation is performed starting from the initial solution at  $t^+ = 16$  over more than 15 additional eddy turn-over times considering the reaction terms. The temporal evolution of the turbulent flame is then statistically characterized by quantifying the consumption speed, the surface area and the front position. Making the assumption that the turbulent flame brush is perpendicular to the x-axis, the overall turbulent consumption speed  $S_T$  and the overall filtered consumption speed  $S_T^*$  are given by:

$$S_T(t) = \frac{1}{\rho_u L_y} \int_0^{L_y} \int_{-L_x/2}^{L_x/2} \rho \dot{\omega}_c(x, y, t) dx dy \quad (13)$$

$$S_T^*(t) = \frac{1}{\rho_u L_y} \int_0^{L_y} \int_{-L_x/2}^{L_x/2} \overline{\rho \dot{\omega}_c(x, y, t)} dx dy. \quad (14)$$

Similarly, the flame surface  $A_T$  and the resolved flame surface  $A_T^*$  are estimated by:

$$A_T(t) = \int_0^{L_y} \int_{-L_x/2}^{L_x/2} |\nabla c(x, y, t)| dx dy, \quad (15)$$

$$A_T^*(t) = \int_0^{L_y} \int_{-L_x/2}^{L_x/2} |\nabla \tilde{c}(x, y, t)| dx dy. \quad (16)$$

As in Fig. 3, the flame front position can be calculated by averaging the axial position values for  $0.4 < \tilde{c} < 0.6$ . DNS2LES results for the temporal evolution of the turbulent flame speed, the turbulent flame surface and the flame front position considering both the NO MODEL and the BOGER closures are compared in Fig. 4 to the reference filtered DNS results. Time-averaged results obtained for  $16 < t^+ < 34$  are also reported in the legend of Fig. 4. First, by looking at results for  $t^+ < 16$  it is possible to understand how the flame establishes and stabilizes once it starts to interact with the turbulent flow. As already said, a laminar flame is initially located at  $x = 0$ . A turbulent flow is injected at the inlet starting at  $t^+ = 0$ .

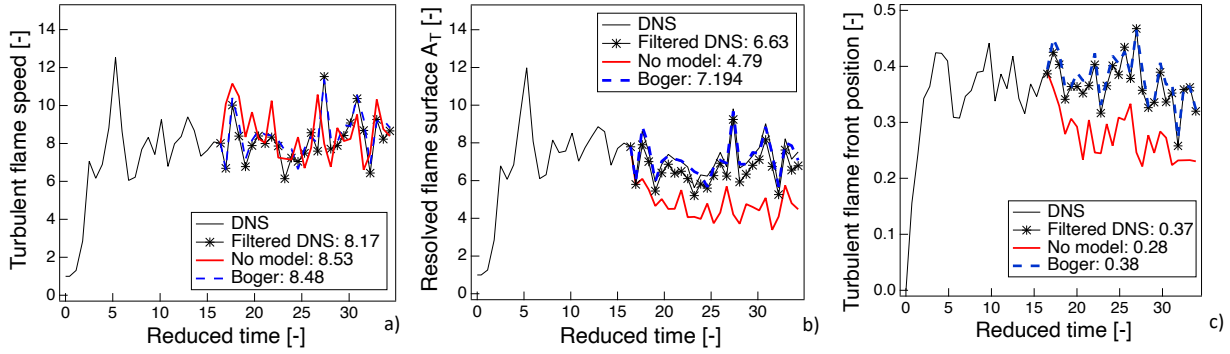


Figure 4: Temporal evolution of the mean resolved flame front characteristics. The turbulent flame speed, flame surface and flame position have been made non-dimensional using  $S_L$ ,  $L_y$  and  $L_x$ , respectively.

Then, the flame front starts to be pushed downstream by the high bulk velocity of the flow (Fig. 4c). At the same time, the flame front is wrinkled by the eddies of the flow so that its flame surface increases of almost a factor 7 (Fig. 4b), consequently increasing the consumption flame speed of the turbulent flame (Fig. 4a). At approximately  $t^+ = 5$ , the turbulent consumption speed balances the displacement imposed by the turbulent flow so that the turbulent flame front finally stabilizes close to the middle of the domain. Even if temporal oscillations on these quantities are observed due to the turbulent nature of the configuration, it is clear that the flame has reached a stationary state for  $t^+ > 5$ . To evaluate the performances of the two considered SGS closures for the source terms, DNS2LES results have to be compared to the filtered results from the DNS. Globally, the BOGER model (dashed blue line) predicts a similar turbulent flame in terms of consumption speed, surface and position so that it can be considered as a good candidate for the subgrid scale closure. On the contrary, the NO MODEL closure (red bold continuous line) does not reproduce the same statistical behaviour of the flame. Indeed, it can be observed that initially the turbulent flame speed is overestimated. Therefore, the flame goes back toward the inlet and stabilizes upstream compared to the reference flame (Fig. 4c). At this position, the flame surface is less wrinkled by the turbulent flow (Fig. 4b). Overall, neglecting the subgrid scale effects seems to affect the localization of the turbulent flame front.

In order to confirm the observed tendencies, statistics have been collected over the last 8 eddy turn-over time on the  $L_x \times L_y$  region illustrated in Fig. 2. The y-mean of the time-averaged fields for the progress variable and the reaction rate as well as the rms reaction rates are considered in Fig. 5. It is possible to identify the effect of the filtering by comparing the DNS results to the filtered DNS results. The time-averaged profiles are identical by construction [23]. A smaller level of fluctuations (of approximately 30%) is observed for the filtered reaction rate compared to the unfiltered one, as expected. Considering the two different closures, the BOGER model provides a good agreement with the reference filtered DNS for both time-averaged and rms quantities, qualifying once again as a good SGS model candidate. On the contrary, as already deduced from Fig. 4, the NO MODEL closure leads

to an incorrect localization of the turbulent flame front, which is also thinner compared to the reference solution. A higher value of the time-averaged reaction rate as well of its fluctuations are also observed with the NO MODEL closure.

This analysis corroborates the need for subgrid closures for reactive scalars. Even for a small filtering factor of the flame front, not accounting for subgrid correlations for the filtered reaction rates leads to an incorrect statistical characterization of the turbulent flame. As expected, the NO MODEL closure burns too fast and it is less wrinkled by the turbulent front. Concerning the Boger's flamelet closure, it was proven in *a posteriori* way that it is a good candidate to reproduce the global characteristics of a turbulent premixed flame such as its consumption speed.

Even if conclusions on the performances of the two considered SGS closures were expected, the obtained results prove the feasibility of the proposed strategy and its interest in evaluating in *a posteriori* straightforward way the validity of SGS models.

## 5. Conclusion

A novel approach for validating subgrid scale model have been investigated. By applying an explicit filtering of the sole species mass fraction equations  $\tilde{Y}_k$ , while keeping fully resolved the flow information, the new strategy allows to focus on the modelling of the filtered scalar term while using fully resolved information for all other fields. To demonstrate the feasibility of the proposed strategy, the resolution of the interaction of a reactive scalar equation with a turbulent flow field has been considered, focusing on the filtered reaction rates. Two different subgrid closures for the reaction rates have been tested. The first one corresponds to a no model for SGS whereas the second case allowed to test the flamelet assumption classically used in flame surface density concepts. The impact of these closures on the statistical characteristics of the turbulent flame (consumption speed, surface and localization) has been quantified in *a posteriori* way.

In further steps, the effects of subgrid models for the different unresolved terms could be evaluated one by one. In addition, it may be of interest to jointly evaluate them since their combination may lead to an increase (or de-

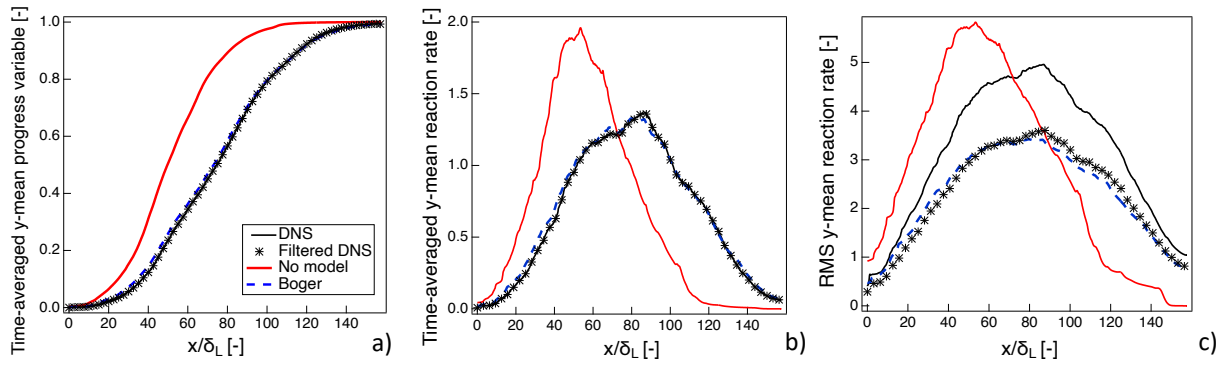


Figure 5: Y-mean spatial profiles of the turbulent flame. The reaction rate has been made non-dimensional using  $\rho_u S_L / \delta_L$ .

crease) of the final errors. Finally, the strategy could be extended to account for the possible retro-coupling of the effects of the subgrid scale models for the transported filtered variables on density and thermal expansion.

### Acknowledgments

This work was granted access to the HPC resources of CINES under the allocation A0052B10294 made by GENCI and of the mesocentre computing center of CentraleSupélec and Ecole Normale Supérieure Paris-Saclay supported by CNRS and Région Ile-de-France. This work has received the European Research Council (ERC) support under the European Union Horizon 2020 research and innovation programme (grant agreement No. 757912).

### References

- [1] D. Veynante, L. Vervisch, *Progress in Energy and Combustion Science* 28 (2002) 193 – 266.
- [2] M. Boger, D. Veynante, H. Boughanem, A. Trouvé, *Proc. Combust. Inst.* 27 (1998) 917–925.
- [3] M. Ihme, H. Pitsch, *Combust. Flame* 155 (2008) 70–89.
- [4] N. Chakraborty, R. S. Cant, *Combust. Flame* 158 (2011) 1768–1787.
- [5] E. R. Hawkes, O. Chatakonda, H. Kolla, A. R. Kerstein, J. H. Chen, *Combust. Flame* 159 (2012) 2690–2703.
- [6] N. Chakraborty, R. S. Cant, *Proc. Combust. Inst.* 34 (2013) 1347–1356.
- [7] D. Veynante, V. Moureau, *Combust. Flame* 162 (2015) 4622–4642.
- [8] S. Lapointe, G. Blanquart, *Combust. Flame* 176 (2017) 500–510.
- [9] M. Klein, N. Chakraborty, *Combust. Sci. Tech.* 191 (2019) 95–108.
- [10] E. R. Hawkes, S. R. Cant, in: *28th Symp. (Int.) on Combustion*, The Combustion Institute, Pittsburgh, 2000, pp. 51–58.
- [11] P. Poinso, D. Veynante, *Theoretical and Numerical Combustion*, e-learning@CERFACS, Third Edition, 2012.
- [12] R. Mercier, V. Moureau, D. Veynante, B. Fiorina, *Proc. Combust. Inst.* 35 (2015) 1359–1366.
- [13] M. Boger, D. Veynante, in: *Eighth European Turbulence Conference*, Barcelona (2000).
- [14] O. Colin, F. Ducros, D. Veynante, T. Poinso, *Physics of Fluids* 12 (2000) 1843–1863.
- [15] F. Charlette, C. Meneveau, D. Veynante, *Combust. Flame* 131 (2002) 159–180.
- [16] V. Moureau, P. Domingo, L. Vervisch, *Combust. Flame* 158 (2011) 1340–1357.
- [17] P. Domingo, L. Vervisch, *Combust. Flame* 177 (2017) 109–122.
- [18] P. Van Cittert, *Z. Phys.* 69 (1931) 298–308.
- [19] Z. M. Nikolaou, L. Vervisch, *Flow, Turb. and Combustion* 101 (2018) 33–53.
- [20] Q. Wang, X. Zhao, M. Ihme, *Combust. Flame* 207 (2019) 89–100.

- [21] O. Colin, M. Rudgyard, *Journal of Computational Physics* 162 (2000) 338–371.
- [22] S. Stolz, N. A. Adams, *Phys. Fluids* 11 (1999) 1699–1701.
- [23] D. Veynante, R. Knikker, *J. Turb.* 7 (2006) 1–20.

